Review of Scientific Instruments

An investigation into experimental *in situ* scanning electron microscope (SEM) imaging at high temperature

Cite as: Rev. Sci. Instrum. **91**, 063702 (2020); https://doi.org/10.1063/1.5144981
Submitted: 13 January 2020 . Accepted: 15 May 2020 . Published Online: 04 June 2020

Rhiannon Heard, John E. Huber, Clive Siviour, Gary Edwards, Ed Williamson-Brown, and Kalin Dragnevski

Review of Scientific Instruments ARTICLE scitation.org/journal/rsi

An investigation into experimental *in situ* scanning electron microscope (SEM) imaging at high temperature

Cite as: Rev. Sci. Instrum. 91, 063702 (2020); doi: 10.1063/1.5144981
Submitted: 13 January 2020 • Accepted: 15 May 2020 •
Published Online: 4 June 2020

Rhiannon Heard,[1,a)] John E. Huber,[1] Clive Siviour,[1] Gary Edwards,[2] Ed Williamson-Brown,[2] and Kalin Dragnevski[1]

AFFILIATIONS

[1]Solid Mechanics Group, Department of Engineering Science, University of Oxford, Parks Road, Oxford OX1 3PJ, United Kingdom
[2]Deben United Kingdom Ltd., Brickfields Business Park, Old Stowmarket Road, Woolpit, Bury St Edmunds, Suffolk IP30 9QS, United Kingdom

[a)]**Author to whom correspondence should be addressed:** rhiannon.heard@trinity.ox.ac.uk

ABSTRACT

This paper presents an investigation into high temperature imaging of metals through the use of a novel heat stage for *in situ* Scanning Electron Microscopy (SEM). The results obtained demonstrate the benefits and challenges of SEM imaging at elevated temperatures of up to 850 °C using Secondary Electron (SE) and Electron Backscatter Diffraction (EBSD) detectors. The data collected using the heat stage demonstrate good beam, vacuum, and detector stability at high temperatures without the need for shielding or detector modification owing to the heat stage geometry. SE imaging highlighted one possible application: carrying out thermal etching, a process in which surface grooves form along a material's grain boundaries during heating *in situ*. The data suggest that using the heat stage to perform imaging during the process gives a more accurate representation of a material's microstructure at temperature than examining the thermally etched specimen after cooling. This study also highlights some of the challenges of high temperature *in situ* EBSD imaging in both steel and nickel at a variety of temperatures and time scales. In particular, the data demonstrate the effect of surface roughness on EBSD imaging and how microstructural changes during heating may affect this. Additionally, the ease with which a material can be imaged using EBSD at temperature may be affected by the material's magnetic properties. For the first time, it is shown that at temperatures close to the Curie temperature of ferromagnetic materials, in this case Nickel, there is a loss of EBSD image quality. Quality was regained when temperatures were further increased. Despite these challenges, good quality EBSD scans were produced, further highlighting the benefits of *in situ* testing for providing information on grain boundaries, orientations, and phase change at elevated temperatures.

I. INTRODUCTION

The development of new experimental methods for micro-scale examination at elevated temperatures facilitates increased understanding of materials that are used in aggressive environments, such as the aerospace and nuclear power industries, and changes during high temperature processing. In particular, the use of Scanning Electron Microscopy (SEM) at high temperatures has enabled observation of changes in grain size and phase during heating.[1] These microstructural features, in turn, dictate the physical and mechanical properties of materials on a macro-scale.

Early reports of *in situ* SEM imaging at elevated temperature combined a Phillips Electroscan ESEM 2020 and purpose built Electroscan hot stage. The stage used electrical resistance heating of a platinum sample holder to observe metals at a temperature up to 1000 °C. The development of this new technology facilitated *in situ* studies on the oxidation of iron by observing the formation of oxide layers within an SEM.[2] The technology also enabled examination of metal dusting corrosion of nickel using a Secondary Electron (SE) detector.[3] More recent *in situ* observations have used electrical resistance heating combined with Electron Backscatter Diffraction (EBSD) imaging. These purpose built *in situ* heaters have allowed

successful capture of grain boundary migration during recrystallization of a thin tantalum ribbon at temperatures between 750 °C and 1030 °C.[4] Tantalum was used owing to its excellent thermal conductivity and its single phase bcc grain structure (which is ideal for EBSD imaging). The same apparatus was subsequently modified for grain growth studies of other materials by spot welding samples to the tantalum ribbon and heating the sample via heat conduction.[4] The electrical resistance heating combined with spot welding greatly reduces the temperature gradient across the sample; however, it also results in the heater being single use.

In order to produce heaters that can be used multiple times, alternative studies have made use of a laser powered heating stage designed for high vacuum applications in a scanning electron microscope at temperatures up to 1000 °C[5] to study phase transformations in steel using EBSD and SE imaging.[1] Similarly, reusable ceramic plates have been used for conductive heating of specimens.[6] Here, *in situ* SEM/EBSD observation of the alpha/gamma phase transformation in Fe–Ni alloys was performed using a purpose built ceramic heating plate, combined with shielding, that operated up to temperatures of 730 °C within a Hitachi Field Emission Gun-SEM (S4200) equipped with an Orientation Imaging Microscopy (OIM) analysis system from TSL.[6]

Commercially available, standalone heating stages have also been developed to facilitate further studies of metals and alloys. Example applications include the demonstration of interphase boundary motion of the ferrite–austenite–ferrite phase change using EBSD maps at temperatures up to 860 °C.[7] In this particular study, low resolution EBSD scans were taken. The scan time had to be less than 100 s at temperatures above 800 °C, owing to the temperature of the EBSD detector phosphor screen exceeding 120 °C (the maximum EBSD detector operating temperature). To prevent this, the detector was retracted to cool between scans. Commercially available stages have further been combined with backscattered imaging of nickel superalloys to capture slip band movement under loading at temperatures up to 750 °C.[8]

The current literature indicates that high temperature Scanning Electron Microscopy (HT-SEM) is a powerful tool for the observation of dynamic crystallographic and microstructural processes in metal alloys, with studies detailing these processes in steel and nickel. In addition to providing heat to the specimen, as discussed above, the technical challenges of heating to high temperature include preventing loss of vacuum, heating of detectors, and degradation of the heating element and minimizing temperature gradients through the sample. The literature also describes further physical challenges associated with imaging at high temperatures. An example of this is the effect of thermionic emission of electrons from heated samples on the signal to noise ratio from the detector.[9] It is noted that EBSD imaging is particularly challenging at high temperatures owing to the close proximity of the detector to the sample and thus possible damage to the detector phosphor screen, the temperature of which typically must not exceed 120 °C.[7] Currently, stage design predominantly focuses on the use of shielding and single use heaters to produce EBSD and SE data. Shielding is used to surround the sample in a furnace-like environment, minimizing temperature gradients while protecting the detectors from radiative heat. The limitations of shielding are that it decreases the visible imaging area and may also cause damage to the specimen surface, which can prevent collection of EBSD data. Furthermore, it may also limit the working distance. Single use heaters, where specimens are spot welded to the heater, are very effective at minimizing the temperature gradient by providing direct contact between the heater and the specimen, facilitating good conduction. However, as well as being consumable and thus potentially expensive to the user, these also prohibit the testing of any electrically non-conductive samples. These solutions have been implemented to some extent in the literature, but there is a lack of studies documenting the impact of the heaters on their surroundings within the SEM, as well as the effect of specific material properties on the ability to image using EBSD at high temperature.

This paper will first describe the development of a novel heat stage with the ability to be used *in situ* to enable imaging in both SE and EBSD configurations without the need for shielding or consumable heaters. Subsequently, it will demonstrate the heat stage's stability within the SEM environment, including the impact on other detectors. Furthermore, material studies on nickel, for which, despite studies at 800–900 °C,[10] EBSD data at temperatures between 200 °C and 600 °C are not available, and steel will show some of the material properties that can impact the ability to image using EBSD over specific temperature ranges and time periods, as well as highlighting some of the benefits of high temperature SEM imaging.

II. METHOD

A. Experimental setup

A series of experiments was conducted using a purpose-built heat stage, shown in Fig. 1, designed in collaboration between the Laboratory for *In situ* Microscopy and Analysis (LIMA) at The University of Oxford and Deben UK Limited. The heat stage is based on a HeatWave® Labs UHV Button Heater, Model 101136, combined with a purpose built mounting and cooling and temperature control system. The heater, an 8 mm diameter molybdenum cylinder, was chosen owing to its high temperature capability of up to 1200 °C, its precision and stability, and the ease of sample mounting. The heater was mounted on a specially designed holder that consisted of brass heat shielding, as well as appropriate mounting fixtures to attach to a Zeiss EVO SEM stage at 70° tilt for Electron Backscattered Diffraction (EBSD) imaging. The proportional-integral-derivative (PID) temperature controller was designed around the use of a K-type thermocouple, which was inserted into the heater holder to make contact with the base of the heater. The stage was purpose built for EBSD imaging by optimizing the working distance between the sample and both the gun and the EBSD detector. To reduce the need for shielding, the geometry of the stage allowed the specimen to completely cover the exposed heater area. Vent holes were added to the casing to minimize vacuum pump down time and maintain vacuum by allowing continuous degassing of the stage during imaging. An adapter was also developed to fix the heat stage in a horizontal position for Secondary Electron (SE) and Backscattered Electron (BSE) imaging.

B. SEM environmental studies

Before performing experiments on specimens, validation experiments were performed to establish the temperature increase in the neighboring detectors within the SEM during heating. This was particularly important as the EDX, EBSD, and BSE detectors have

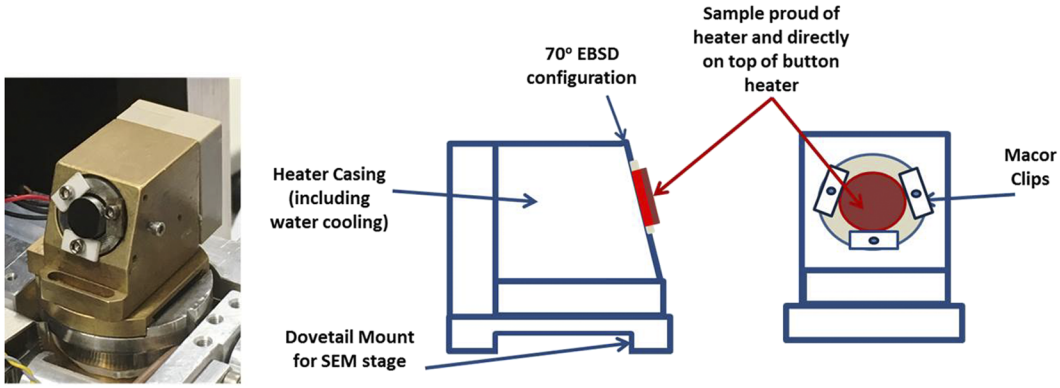

FIG. 1. Heat stage accompanied by a schematic showing key features.

low maximum operating temperatures of 50 °C, 120 °C, and 300 °C, respectively.[7] K-type thermocouples were attached to the electron gun column and EBSD detector using small Carbon tabs (Fig. 2) and to the outer surface of the heat stage using Macor® clips. The heat stage was heated up to 850 °C and held for 2 h in its EBSD position. The temperatures of the heat stage and detectors were monitored and recorded over this time period using a Pico Technology TC-08 Thermocouple Data Logger sampling at a rate of 1 Hz. Note that, during elevated temperature tests, the EDX detector was fully retracted out of the chamber owing to its very low maximum operating temperature of 50 °C. All EDX data detailed in this paper were obtained at room temperature.

Further temperature validation experiments were conducted with an industrially pure nickel specimen, ~1 mm thickness, and 8 mm diameter to quantify the surface temperature of the specimen compared to that of the heater. Data were recorded every second from a K-type thermocouple mounted on the nickel sample surface during heating and after equilibrium was achieved. Data were compared to the heat stage set temperature and to analytical calculations performed using Fourier's Law of heat conduction,

$$\dot{Q} = -kA\frac{T - T_1}{\Delta x}, \tag{1}$$

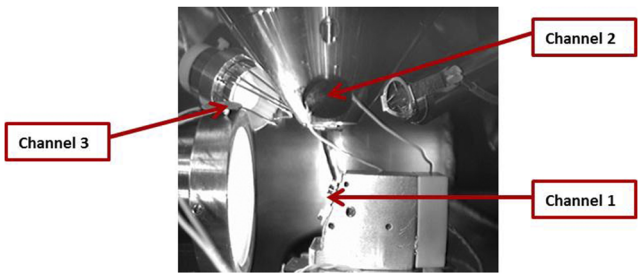

FIG. 2. Experimental setup for SEM detector and environment thermocouple measurements. Readings were taken at the heat stage surface (channel 1), on the gun (channel 2), and on the EBSD detector (channel 3).

and the Stefan–Boltzmann law,

$$\dot{Q} = \varepsilon A\sigma T^4, \tag{2}$$

assuming that the only heat loss from the specimen is radiation from the surface. Here, A is the specimen face surface area (m^2), Δx is the thickness of the specimen (m), $\dot{Q}$ is the heat flux from the specimen free surface (W), κ is the thermal conductivity of the specimen (50 W m^{-1} K^{-1}), ϵ is the emissivity of the specimen, σ is the Stefan–Boltzmann constant (5.67×10^{-8} W m K^{-4}), T is the specimen top surface temperature (K), and T_1 is the heat stage temperature (K). Setting the heat flux due to conduction equal to the radiated heat provides the steady state surface temperature. This calculation neglects conduction and convection, which seems a reasonable assumption given the high vacuum environment within the SEM.

C. Investigative high temperature imaging

To investigate the EBSD imaging ability at high temperatures using the heat stage, industrially pure nickel (99.5% Ni) specimens were selected as a reference due to nickel's use in the calibration of EBSD detectors.[11] Nickel is used in this capacity due to its high orientation and high topographic contrast from polishing, which make it ideal for EBSD imaging.[12] Disk samples of nickel with a diameter of 8 mm were initially ground using progressively finer silicon carbide papers (grades: P240, P400, P600, P800, P1200). Samples were then polished, first using three grades of diamond suspension (9 μm, 3 μm, 1 μm) and finally colloidal silica (0.07 μm) combined with a water-based lubricant, down to a thickness of ~1 mm. The nickel was mounted on the stage using Macor clips, which were designed to align the sample in the center of the stage without touching the sample surface. This mounting procedure avoided shadowing or damage to the polished specimen.

The nickel specimen was heated up to 800 °C (just below the maximum of the heating stage) with scans recorded at 100 °C intervals. EBSD scans over 40×115 μm^2 regions were taken after 5 min of heating at each temperature using a raster step size of 0.5 μm. Each scan was completed in 3–4 min and taken in approximately the same location. Once the series of EBSD scans at 100 °C temperature intervals were complete, a large scan of 250×700 μm^2 at a step size of

1 μm was carried out at 850 °C, which took 1.5 h to complete. To further investigate the heat stage's stability, SE images were also captured during heating to observe any changes in the nickel surface with temperature and time. The SE images were taken at a magnification of 650× again at 100 °C intervals up to 800 °C, at 850 °C, and upon cooling at room temperature. The magnification is a compromise between the need to capture enough grains for analysis and the need to perform the scan in less than 5 min to minimize the adverse effects of beam drift.

Similar experiments were carried out on 0.4% carbon steel as an example application study, with EBSD imaging at 850 °C. The sample had the same dimensions as the nickel sample and underwent a similar grinding and polishing process. Phase change and grain development at these temperatures were monitored using EBSD imaging. Scans at 850 °C were of sizes 2 × 40 μm^2 and 20 × 50 μm^2, both with step size 0.2 μm. Scans at temperatures between 100 °C and 800 °C were 30 × 60 μm^2 in size. The EBSD scans took between 2 min and 5 min each to complete and scan times and magnifications were selected for similar reasons as for the nickel data.

D. Temperature impact on EBSD surface quality

To image using EBSD, a very smooth, polished surface is required. The level of surface roughness at which EBSD data can be captured is dictated by the material interaction volume. Material interaction volume is defined as the elastic mean free path of electrons,[13] which is a measure of the depth to which the electrons penetrate the material surface. This can be calculated for elements using the Kanaya–Okayama range equation[14] or can be simulated for elements, alloys, and compounds using a Monte Carlo simulation known as CASINO.[15] CASINO is a single scattering Monte Carlo Simulation of electron trajectory in a solid, specially designed for low-beam interaction in bulk and thin foil specimens and shows good agreement with the Kanaya–Okayama range equation. The program can be used to generate all recorded signals (x rays and secondary and backscattered electrons) in an SEM for the acceleration voltages 0.1–30 kV.[15] In this study, CASINO was used to estimate the interaction volume for carbon steel and nickel using the trajectories of the backscattered and secondary electrons from the surface through the bulk of the specimen. The CASINO simulation parameters used were 10 000 electrons at a voltage 30 keV (beam voltage used for EBSD imaging) for a bulk sample tilted at 70° (standard angle for EBSD).

The corresponding interaction volume was compared to the roughness and depth profiles of steel and nickel samples before and after heating to supplement the EBSD and SE data and understand the effect temperature may have on sample preparation. The roughness data were documented using Atomic Force Microscopy (AFM) measurements recorded over an area of 50 × 50 μm^2. Measurements were taken both after samples were prepared for EBSD imaging and again after a thermal cycle: heating at 850 °C in 10 min holding for 1 h and cooling to room temperature over 30 min, with three measurements taken each time. EDX scans of the Steel samples were also taken post cooling, but it remained in vacuum, to identify where any oxidation that may have occurred and its resulting effect on image quality.

To determine the effect of heating on the sample surface, the roughness parameters Ra, Rq, and Rmax were compared before and after heating. Ra is the arithmetic average of the absolute values of the profile height deviations (peaks and valleys) from the mean line, while Rq is the root mean square average of the profile heights from the mean. Rmax is the maximum roughness, which is defined as the maximum peak to the valley dimension across the roughness area profiled. The depth distribution of roughness, defined as the percentage of the surface area that is at a given depth (from the topology data taken relative to the maximum height), was also compared, before and after heating, to the depth of the interaction volume.

III. RESULTS

A. Heat stage thermal testing results

During pump down and testing, the vacuum in the chamber was monitored. The pump down time was ~1 h compared to a 3–5 min pump down time for the chamber without the heat stage. After pump down, the chamber pressure was maintained at less than 9×10^{-5} mbar throughout testing of the heat stage, which was comparable to that without the stage. Figure 3 depicts the results of the environmental and detector tests within the SEM. Figure 3(a) shows the surface temperature of the heat stage for 2 h, and the temperature is shown to be constant after the first 30 min. Figure 3(b) shows the corresponding temperature of the EBSD detector and bottom of the gun column during the heating in Fig. 3(a). The detector temperature readings indicate that the detectors do not exceed 45 °C even after holding the stage temperature at 850 °C for 2 h. The temperature of the EBSD detector reaches a plateau at ~100 min, suggesting that thermal equilibrium has been reached and heating over several hours would not cause a significant rise in detector temperature. Thus, based on these results, it is anticipated that *in situ* high temperature imaging could be safely executed over a number of hours without damaging the EBSD or SE detector (based on the location of the thermocouple on the gun column), given that the detector temperatures reach thermal equilibrium during the time period monitored.

The temperature gradient results from the nickel specimen [Fig. 3(c)] show the temperature at the surface of the sample and the set-point temperature of the stage. The data show a 2 °C temperature difference between the heat stage and sample surface once thermal equilibrium is reached. Calculations indicate an expected difference of less than 1 °C across metal samples of 1 mm thickness, the exact value being dependent on the metal. Given potential errors in the temperature measurements (e.g., K-type thermocouples are accurate to within ~2% of the indicated temperature), this is consistent with the data obtained.

B. Results from high temperature EBSD on nickel

A set of 40 × 115 μm^2 EBSD scans of nickel were taken at 100 °C intervals; a schematic of the heating profile is shown in Fig. 4. Once each temperature was reached, the sample was held for 5 min and SE and EBSD images were taken before increasing the temperature to the next interval. Figure 5 shows the nickel inverse pole figure EBSD maps produced. It is noted that the scans are all performed in approximately the same location on the specimen, excluding some slight beam drift; however, the clarity of the EBSD scans at 300 °C

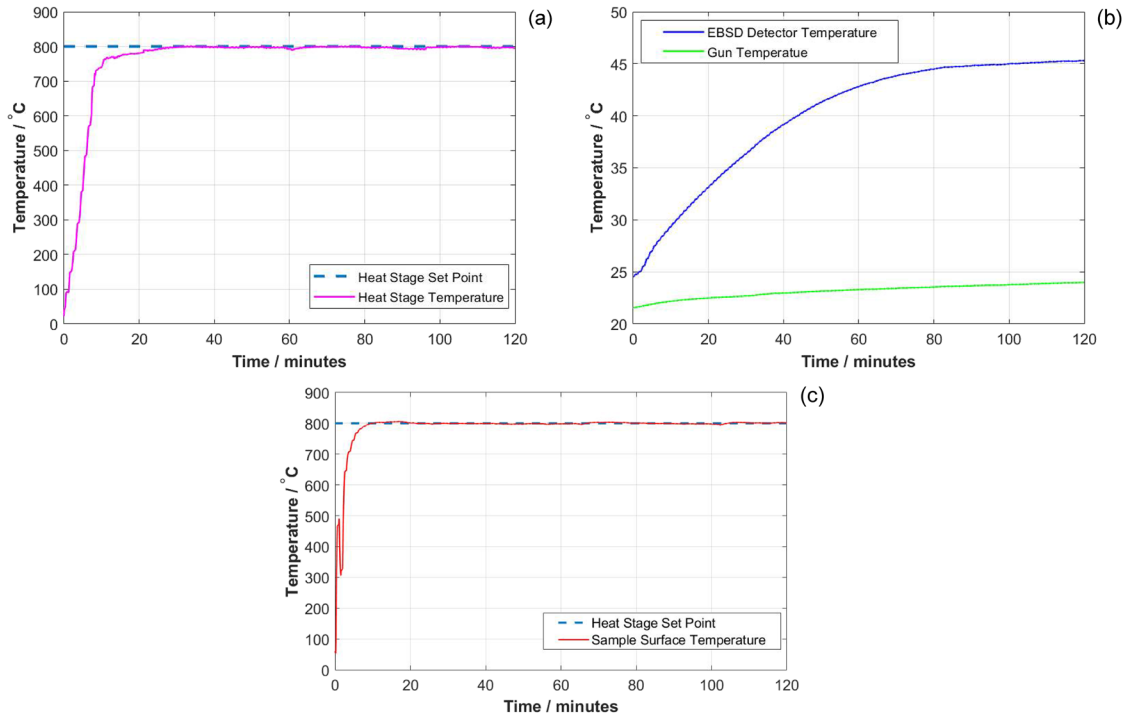

FIG. 3. Results of the temperature testing: (a) Heat stage heating profile and (b) accompanying detector temperatures during heating of the heat stage to 850 °C. (c) Surface temperature of a 1 mm thick nickel specimen heated to a nominal 800 °C.

and 400 °C show significant deterioration compared to the others. It is known that the index-ability of the Kikuchi patterns is dictated by the uniformity of brightness and orientation of the bands;[16] an ideal example is shown in Fig. 6(a). Although a Kikuchi pattern may be easily interpretable by the human eye, they may not be recognizable by the software once they are transformed into Hough Space. Indexable Kikuchi patterns may not be produced if the bands are non-uniform in intensity, i.e., a mix of light and dark, as shown in the 300 °C Kikuchi patterns, indicated in Fig. 6(b). Similarly, if the bands are significantly blurred as they are at 400 °C [Fig. 6(c)], this may impair the Hough transform's accuracy, accounting for a loss of EBSD image quality at this temperature.

The EBSD pattern quality can be quantified by two main parameters: the Fit and Confidence Index (C.I.). The fit is defined as the average angular deviation between the recalculated bands and the detected bands.[1,11] An ideal Fit is as small as possible but is generally accepted as between 0.5° and 2°.[17] The C.I. measures the probability of correctness of an orientation solution relative to other interpretations of the data. A common approach is to calculate the average C.I. across the whole image and only use images with an average C.I. greater than 0.3.[17] Figure 7 shows the C.I. and fit vs temperature for nickel. The data indicate a drop in C.I. below the acceptable level at 300 °C and 400 °C, followed by a return to acceptable levels at higher temperatures. Similarly, scans of all temperatures except 300 °C and 400 °C show an average fit of between 1.2° and 1.4°. However, at temperatures of 300 °C and 400 °C, the fit worsens with a significant increase from 1.2° to about 1.8°. Hence, the reliability of the statistical analysis is reduced and the pattern not indexable.

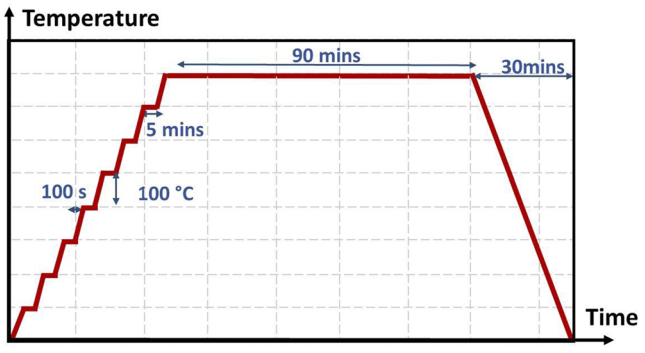

FIG. 4. Schematic of the heating profile of the nickel specimen for all EBSD and SE images taken.

C. Results from high temperature SE imaging of nickel

SE images were also taken at 100 °C intervals during the heating between 100 °C and 800 °C (see Fig. 4 for heating profile). Figure 8 shows the development of grain boundary outlines during heating

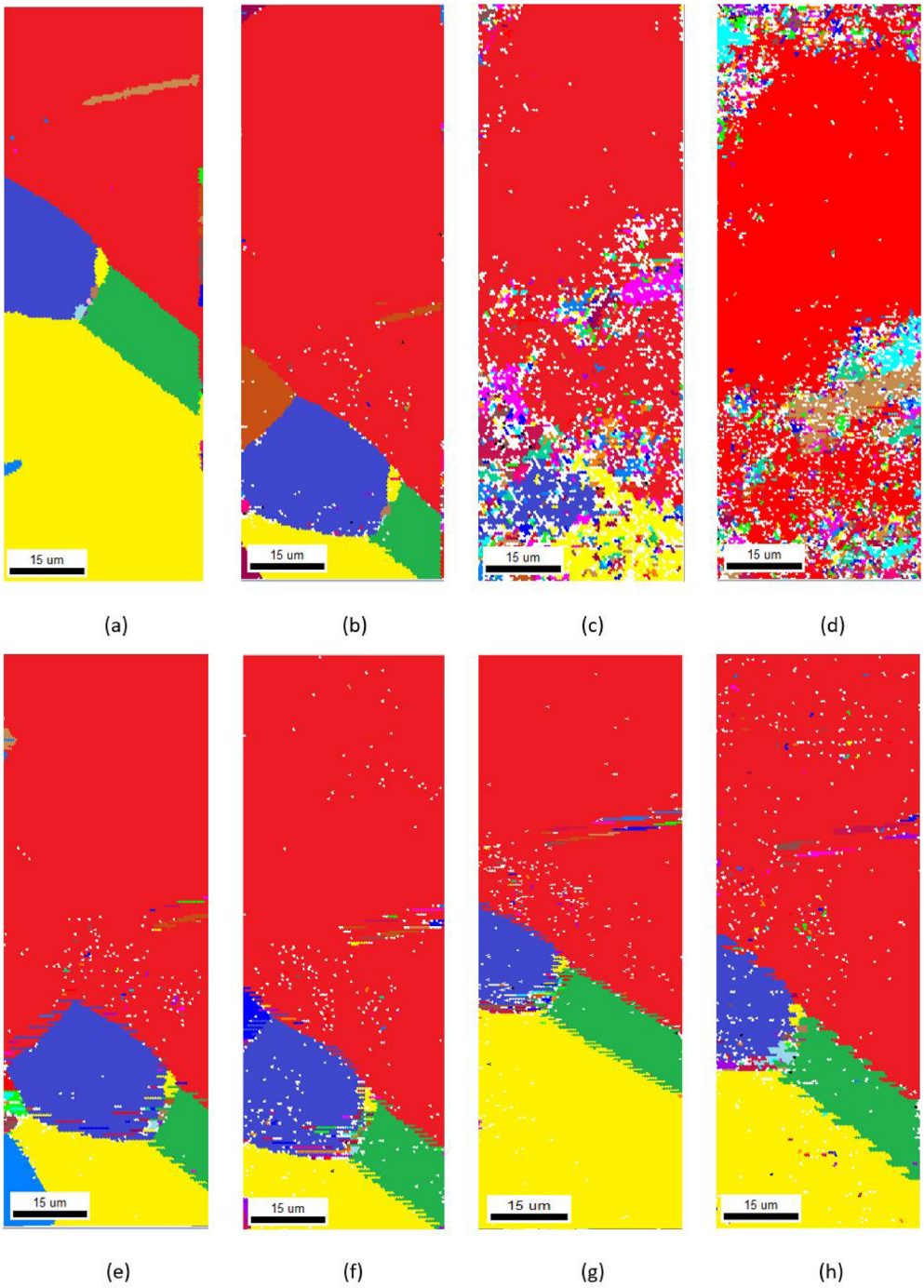

FIG. 5. Raw (uncleaned) grain maps of nickel at temperatures of (a) 100 °C, (b) 200 °C, (c) 300 °C, (d) 400 °C, (e) 500 °C, (f) 600 °C, (g) 700 °C, and (h) 800 °C, demonstrating a significant loss of image quality at 300 °C and 400 °C.

through the temperature intervals and over time: room temperature [Fig. 10(a)], 500 °C [Fig. 10(b)], 700 °C [Fig. 10(c)], and at room temperature after cooling for 30 min from 800 °C [Fig. 10(d)]. The grain boundaries appeared after a total heating time of 40 min (5 min for each previous interval with heating between temperatures taking 100 s) at 700 °C but were not seen at lower temperatures. Once revealed, nickel grain boundaries [see red arrows in Figs. 8(c) and 8(d)] remained visible after cooling. Thee small, rectangular

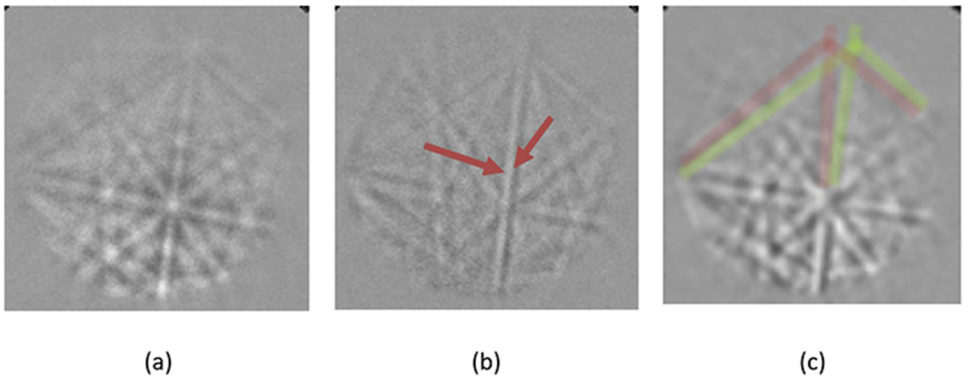

FIG. 6. Sample nickel Kikuchi patterns demonstrating the types of degradation of pattern that can occur. For example, (a) at 200 °C showing uniform bands, (b) at 300 °C showing a loss of uniformity in band intensity, indicated by the arrows where one side of a band is significantly darker than the other, and (c) at 400 °C depicting blurring and duplication of bands at a slightly off angle as highlighted.

darkened regions in the SE images [see yellow arrows in Figs. 8(b) and 8(c)] are due to EBSD beam damage.[18]

D. High temperature steel results

EBSD images of 0.4% carbon steel were also captured at temperatures up to 850 °C, demonstrating an ability to image steel at these high temperatures. For data presented in Figs. 10 and 11, steel was heated to 850 °C in 10 min and held for 60 min; Fig. 9(a) shows a schematic of the temperature vs time profile. Data recorded in Fig. 12 were obtained from a sample heated to 800 °C over a period of 83 min pausing at 100 °C intervals to take SE and EBSD images, as shown in Fig. 9(b).

Figure 10 depicts the EBSD inverse pole figure and phase maps at room temperature and after 10 min of heating at 850 °C shows visible microstructural changes. In particular, Figs. 10(c) and 10(d) show the phase transformation from ferrite (red) and pearlite (green), at room temperature, to austenite (yellow), at 850 °C. However, the speed at which scans must be undertaken as a compromise between beam drift and scan size can impact the scan clarity: here, the scans were captured in less than 3 min. The steel was held at 850 °C to observe the phase change using EBSD, and image quality scans are shown in Fig. 11. The scan quality shows degradation over time, with a significant loss of image quality after 21 min of heating when imaging the same area [Fig. 11(c)].

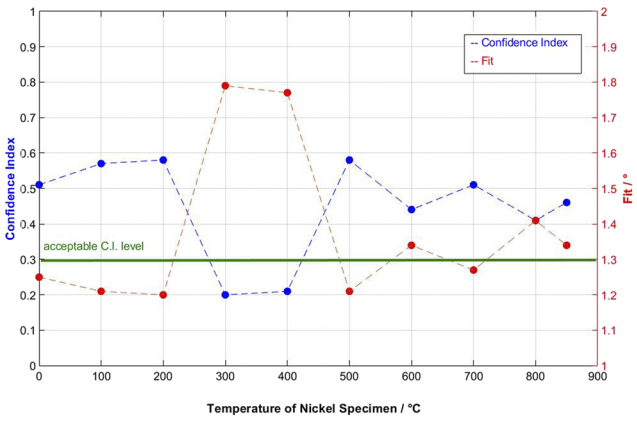

FIG. 7. Confidence Index (C.I.) and fit of the whole scanned area at each temperature showing a significant drop in C.I. in scans at 300 °C and 400 °C to below the acceptable C.I. level of 0.3 (represented by the green line). The plot also shows an increase in the Fit value around these temperatures, suggesting that the Kikuchi patterns are a poor match to those held in the statistical database. Data in this graph correspond to images in Figs. 5 and 6.

Steel samples were also observed during stepped heating using SE and EBSD imaging [see Fig. 9(b) for the heating profile]. The EBSD image quality images, shown in Fig. 12, showed progressively worsening image quality with the increase in time and temperature. However, Fig. 10 has already demonstrated images obtained at 850 °C after rapid heating, when the temperature was increased to 850 °C within 10 min, rather than over a prolonged period as was used for the interval images depicted in Fig. 12.

EDX scans were taken of the samples post cooling after 1 h at 850 °C [heating profile in Fig. 9(a)] to determine the level of oxidation during heating and its possible impact on surface quality. These are shown in Fig. 13. Figure 13 indicates that there are a few small areas of oxidization, attributed to remaining colloidal silica from surface preparation but that most of the sample surface is free from oxygen. To further investigate the difficulty of imaging steel after heating for 1 h at 850 °C, surface topography measurements were carried out using AFM on steel samples before and after heating, shown in Fig. 14. The scans showed a significant increase in the roughness parameters, before heating Ra = 44.1 nm and Rq = 37.4 nm, while after the heating and cooling cycle, Ra = 83.2 nm and Rq = 63.4 nm. The maximum roughness also increased, with the highest values of maximum roughness being 447 nm before heating and 1059 nm afterward.

IV. DISCUSSION

The data obtained demonstrate that imaging at high temperature enables the microstructure of metals to be monitored in real time. Additionally, the SE and EBSD images can be used to highlight several interesting observations, which indicate both the benefits and challenges of imaging at such high temperatures. Further analysis and discussion of the possible uses of these data and causes of the observed features and phenomena are given below.

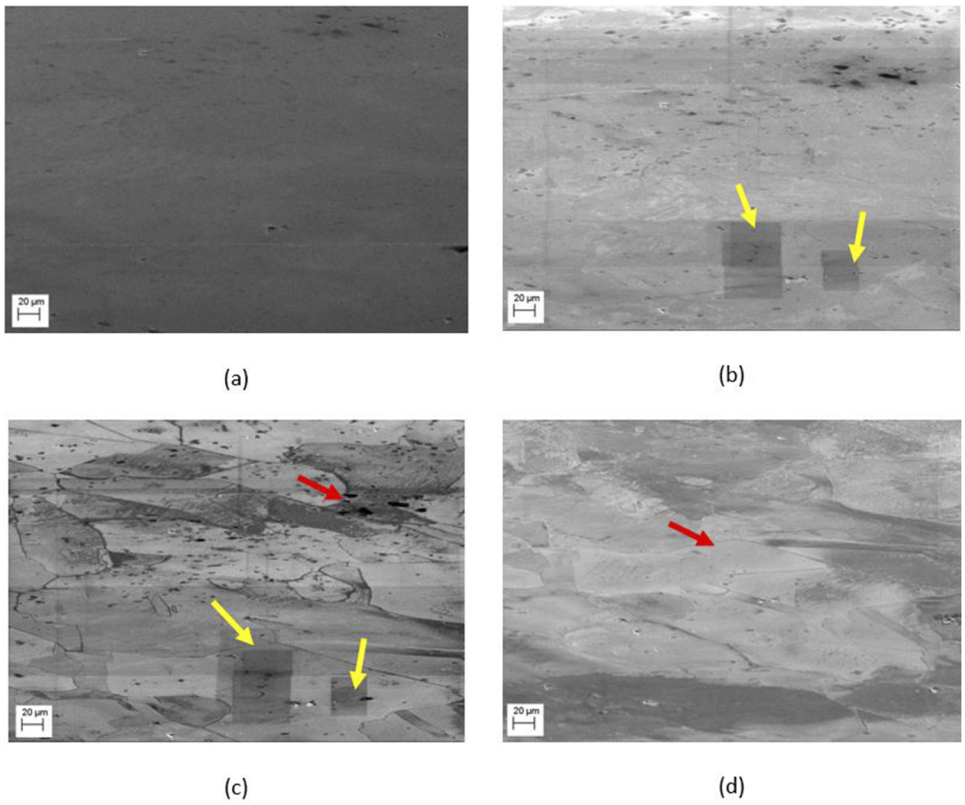

FIG. 8. SE images of a nickel specimen (a) at room temperature before heating, (b) at 500 °C, (c) at 700 °C, and (d) at room temperature after heating with some beam drift. Dark rectangles (see yellow arrows) are from EBSD surface damage. The dark lines are grain boundaries (see red arrows).

A. Heat stage thermal testing

The data demonstrating the effects of holding specimens at elevated temperature on the detectors and SEM environment suggest that detectors will not need to be retracted or removed during testing, except for the EDX detector. Moreover, as the sample surface temperature for a 1 mm thick specimen is almost identical to the heat stage surface temperature, surface mounted thermocouples are not essential for measuring the temperature of the specimen: the data confirm that this can be assumed to be the heat stage set point temperature. This is advantageous in preventing shadowing or loss of surface quality from thermocouple mounting.

B. EBSD image quality degradation: Temperature dependence

A significant degradation in the EBSD scan quality for nickel at 300 °C and 400 °C compared to higher and lower temperatures was observed. This loss is quantified by a drop in confidence index and increase in fit angle at these temperatures. A potential explanation that infrared radiation from the sample interferes with the detector was discounted as neither the phosphor screen nor the CCD camera is sensitive to the wavelengths emitted at a temperature of 300–400 °C. This is attributed to the presence of protective coatings and filters.[10] Furthermore, steel showed no significant change in C.I. or fit at these temperatures, despite having a similar

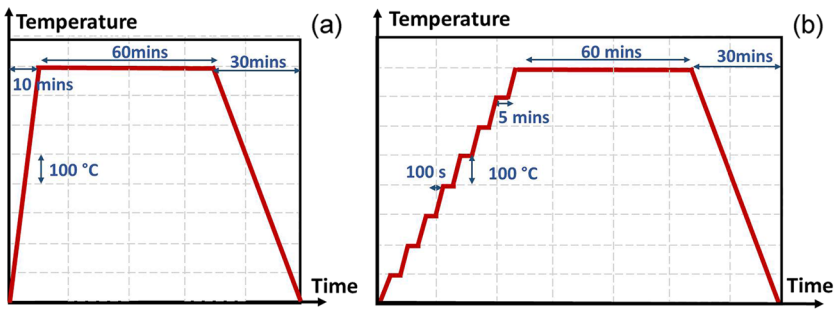

FIG. 9. Schematics of temperature profiles for the two sets of steel data. (a) Temperature profile corresponding to results in Figs. 12 and 13. (b) Stepped temperature profile corresponding to the results in Fig. 12.

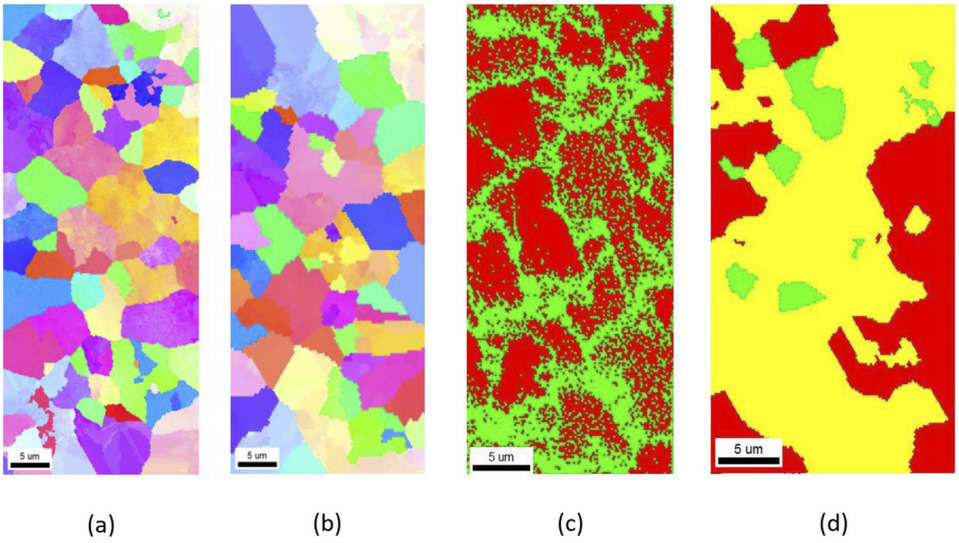

FIG. 10. EBSD IPF maps of 0.4% carbon steel where (a) and (b) show inverse pole figure maps and (c) and (d) show phase maps. (a) and (c) are at room temperature and (b) and (d) are at 850 °C.

emissivity.[19] Hence, this loss of imaging is thought to be dependent on intrinsic material properties.

Nickel is ferromagnetic at room temperature. However, its magnetization is temperature dependent and its susceptibility follows the Curie–Weiss Law,[20] with a Curie temperature, T_c, of ~630 K (~355 °C) above which it is paramagnetic.[21] Nickel's magnetization stays fairly constant from room temperature up to 420 K (~$2/3T_c$, ~150 °C). After this point, magnetization decreases with the increase in temperature, reaching zero at T_c.

Studies on the effect of a magnetic field on SEM imaging indicate that it can have an impact on the ability to image and cause a loss of image intensity. Brodusch *et al.*[16] illustrated the influence of local magnetization on electron trajectories resulting in a change in contrast intensity of backscattered electrons and small shifts in the location and sharpness of Kikuchi bands. Close to the Curie temperature, the nickel sample may be expected to have mixed phases (i.e., mixed paramagnetic and ferromagnetic) with the spatial arrangement of these being easily disturbed by external influences. This may cause a significant loss of Kikuchi pattern intensity, as in the case of the 300 °C Nickel pattern, owing to the spreading out of the interaction volume because of the coexistence of the two magnetic phases close to the Curie point. The slight shifts in Kikuchi patterns attributed to the presence of a magnetic field may also cause blurring or duplication of the Kikuchi bands, as seen in the Nickel Kikuchi patterns at 400 °C, resulting in a low quality EBSD map.

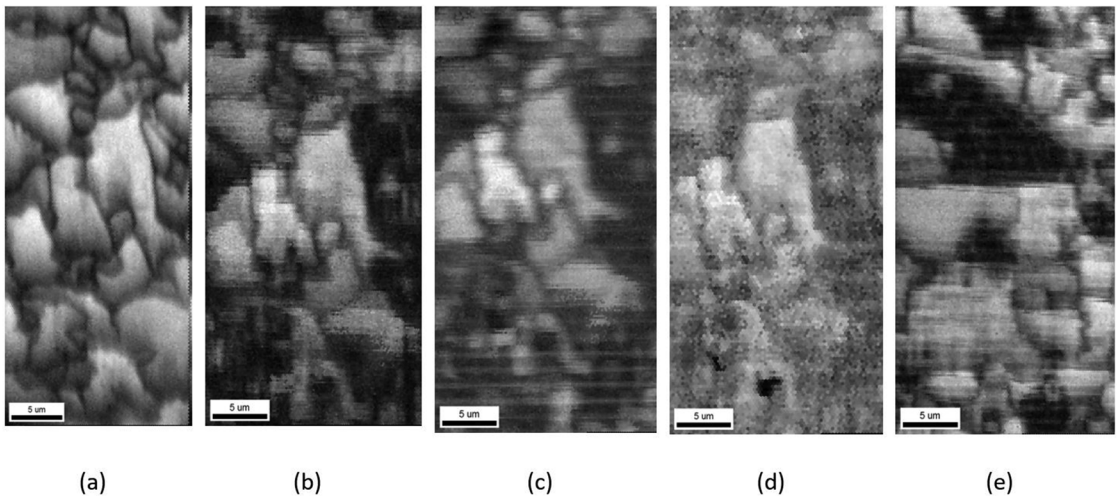

FIG. 11. EBSD image quality maps of the same area after holding at 850 °C for (a) 2 min, (b) 10 min, (c) 21 min, (d) 31 min, and (e) 40 min, showing a significant loss of image quality after 20 min and limited usability of images after this time.

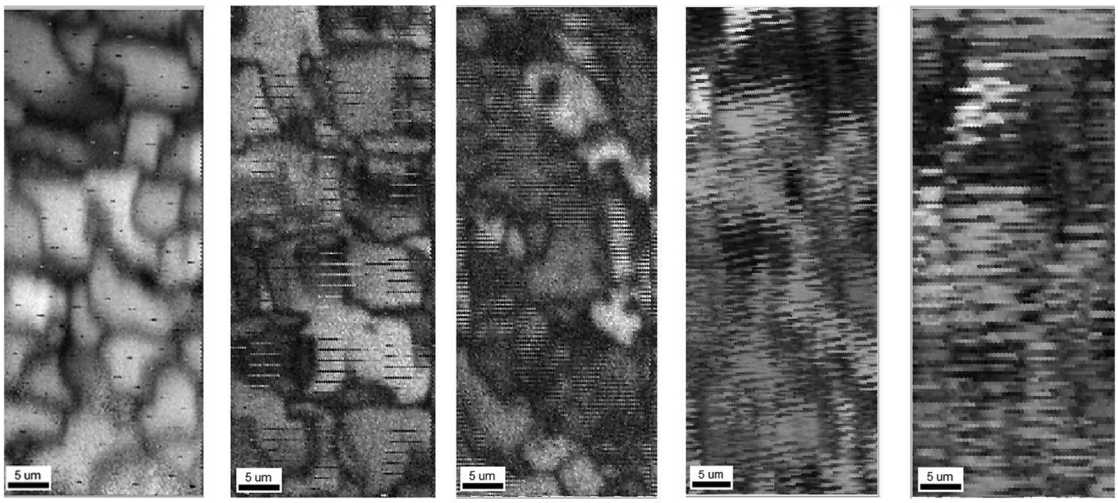

FIG. 12. Image quality EBSD maps of 0.4 wt. % carbon steel at (a) 100 °C, (b) 300 °C, (c) 500 °C (d) 700 °C, and (e) 800 °C of the same surface area showing progressively worsening image quality with the increase in temperature and significant loss at 700 °C and 800 °C. The heating profile is in 3.7 b.

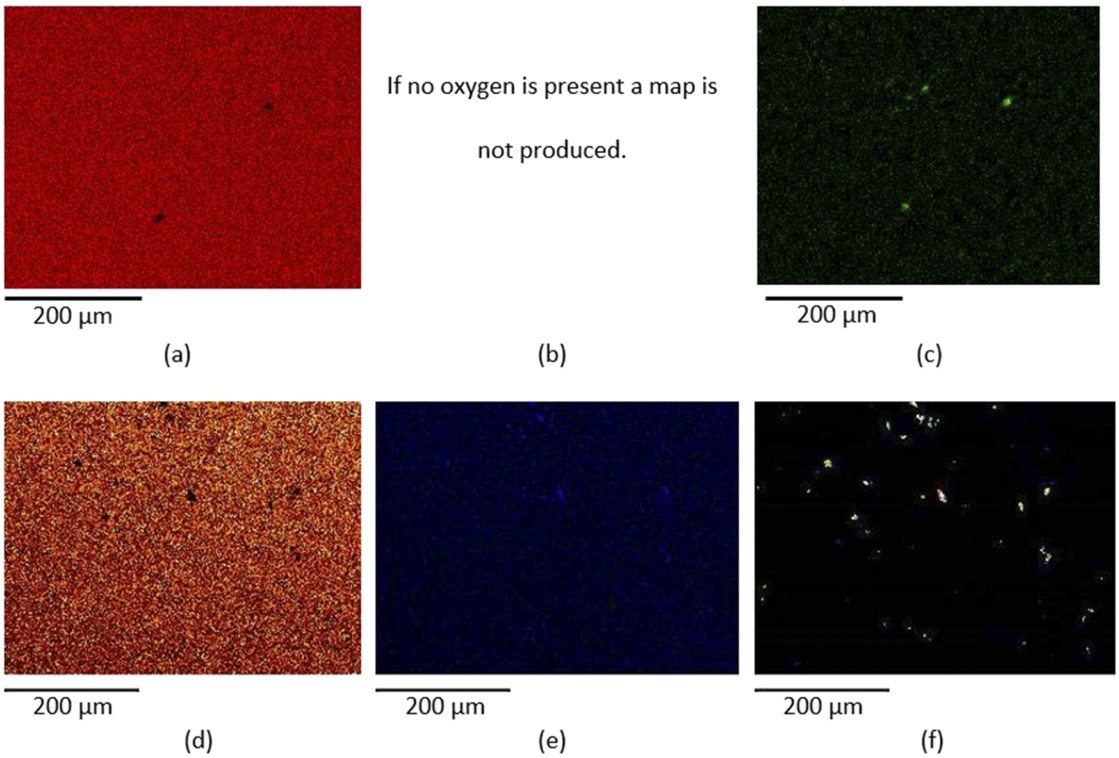

FIG. 13. EDX maps of steel within the SEM [(a)–(c)] before heating and [(d)–(f)] post heating, indicating no detectable oxygen. The EDX elements detected are [(a) and (d)] iron, [(b) and (e)] oxygen, and [(c) and (f)] silicon.

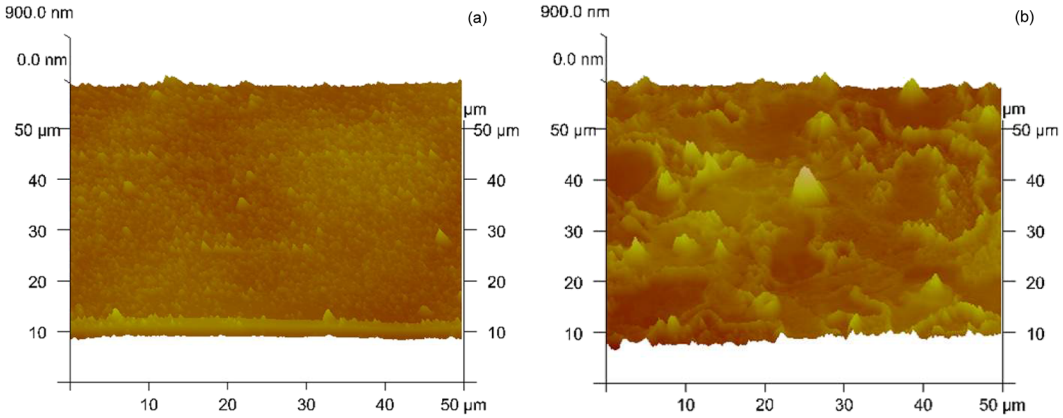

FIG. 14. AFM roughness profiles of steel (a) preheating and (b) postheating.

Steel is also ferromagnetic at room temperature, having a Curie temperature of ~770 °C dependent on alloying.[22] On this basis, degradation of EBSD quality may be expected between 700 °C and 800 °C and indexable patterns to return at about 850 °C. In the present study, a severe degradation of EBSD quality was seen from 700 °C to 800 °C. However, there is also reduced EBSD quality at elevated temperatures that are nevertheless less than 700 °C. This suggests that other factors such as phase changes or loss of surface quality as a result of prolonged heating may be significant.

Overall, the data for Nickel strongly suggest that the quality of the Kikuchi patterns is affected close to the Curie temperature, and this limits the ability to index EBSD data. However, for steel, other factors appear to be significant requiring further explanation; this is discussed below.

C. EBSD image quality degradation: Time dependence

In general, the *in situ* imaging of steel indicates that the speed at which images are taken during phase changes and grain growth may also have an impact on the clarity of the scans. Hence, a very high polish will be required initially, as this has been found to help facilitate good image quality when rapid scans with 0.3–1 μm step size over areas as large as 40 × 90 μm^2 are taken in 2–3 min. Often, high quality scans can take several hours with step sizes of 0.1 μm, while microstructural changes may occur on the timescale of seconds to minutes. Repeated imaging of an area can also lead to visible surface damage of the sample, as shown in Fig. 8, and this can also impact the quality of the scan leading to the necessity for quick scans that are evenly spaced over a time period.

The EBSD scans of steel also showed significant degradation over time during heating at 850 °C. The reasons for this are thought to be either oxidation or an increase in roughness. Oxidation would likely have a negative impact on image quality if an oxide layer constitutes a significant fraction of the sampled volume, as the EBSD detector may then be unable to differentiate the oxide and the steel patterns. However, the EDX scans in Fig. 13 indicate that, in the present study, oxidation is localized, so this does not appear to account for the loss of image quality. EBSD is also dependent on having a smooth diffracting surface to avoid spatial blurring of the Kikuchi patterns. The AFM measurements show a significant increase in roughness during the heat cycle. Thus, the change in surface finish during the heating process may be linked to the loss of image quality of EBSD scans when imaged over a long period of time, as has been observed in these experiments [Figs. 11 and 12].

As mentioned previously, the level of acceptable surface roughness is dictated by the interaction volume.[23] To quantify this, CASINO simulations were run for steel in an EBSD 70° configuration with 10 000 electrons simulated at a voltage of 30 kV. The size of the maximum interaction volume for backscattered electrons is found to be about 940 nm. The distribution of electrons is shown in Fig. 15, which also shows that secondary electrons have a much greater interaction volume than the backscattered electrons.

A comparison of the surface roughness depth profiles before and after heating and the interaction volume depth profile was performed [Fig. 16]. The graph shows the percentage of the surface area that at a given depth (from the topology data taken relative to the maximum height) and the percentage of electrons that penetrate a given interaction volume (interaction volume refers to the depth an electron penetrates; from the CASINO data) for both nickel and steel specimens. The data for steel show that there are a significant number of electrons penetrating the sample at a greater depth than the characteristic depth of the surface topology before heating; however, post heating, the surface roughness is deeper than the penetration depth of nearly all electrons. This is likely to be the cause of the loss of indexable patterns in steel after 20 min held at elevated high temperature; the increase in surface roughness is sufficient to impede the electron–sample interaction required for EBSD. On the other hand, the nickel topology data show that although the roughness increases, it does not increase to a greater depth than the electrons are able to penetrate.

D. SE image grain boundary visibility

The nickel SE images show that the outlines of grain boundaries become visible over time at temperatures above 700 °C; a

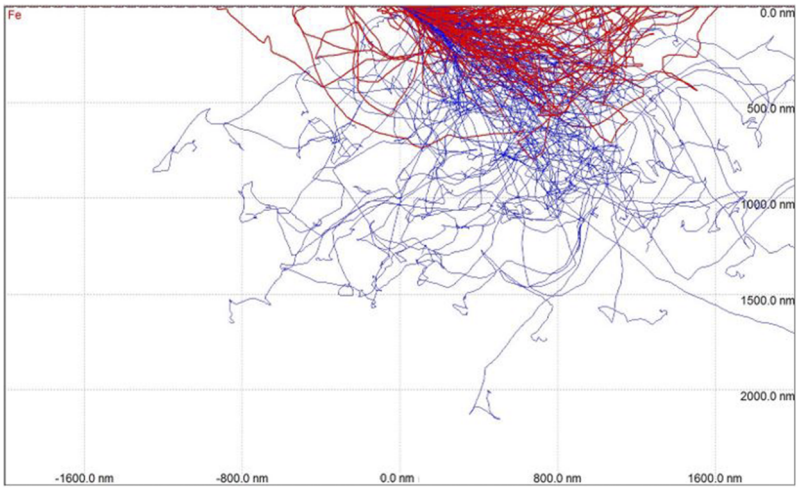

FIG. 15. CASINO simulation for steel at 30 kV showing the interaction volume of depth of primary electrons that will produce backscattered electrons (red path) and secondary electrons (blue path).

phenomenon known as thermal etching. Thermal etching is the development of surface grooves at the grain boundaries through exposure of a polished surface to elevated temperatures. The grain boundaries impinge on the specimen surface, and as a result of thermodynamic equilibration of the triple junction between the grain boundary and the free surface, the specimen surface rises away from the boundary.[24] In this case, *in situ* heating of the nickel demonstrates the formation of thermal etching at around 700 °C and during heating to 800 °C, leading to the etch being retained upon cooling (Fig. 10). The phenomenon of thermal etching of grain boundaries was confirmed by comparing the EBSD and SE images of the same area of nickel at 850 °C, which were found to match with good agreement.

A comparison of the etch as observed in images taken at 850 °C was also made to the SE image taken after cooling along with their respective EBSD image quality maps; these are shown in Fig. 17. The SE images indicate that some change in grain structure occurs during cooling of the grains outlined in white and indicated with

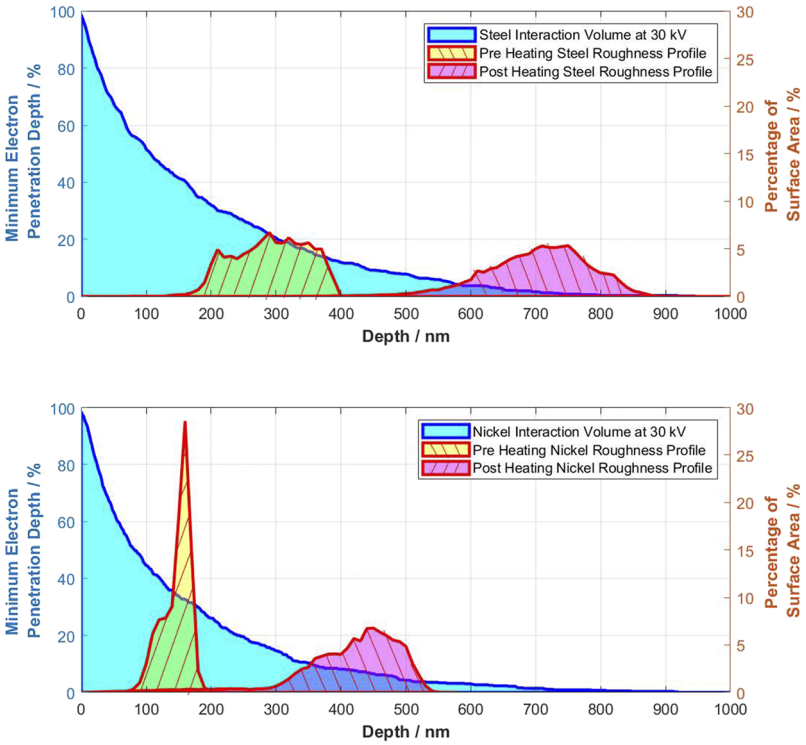

FIG. 16. Surface depth profiles across the 50 × 50 μm^2 scanned area for before heating (yellow and forward slash hatched) and after heating (magenta and back slash hatched) compared to the interaction volume (electron depth penetration) for (top) nickel and (bottom) steel, respectively. The interaction volume is represented by the blue line showing the normalized distribution of the CASINO simulated interaction depths of 10 000 scattered electrons, simulated at 30 kV within the corresponding surface.

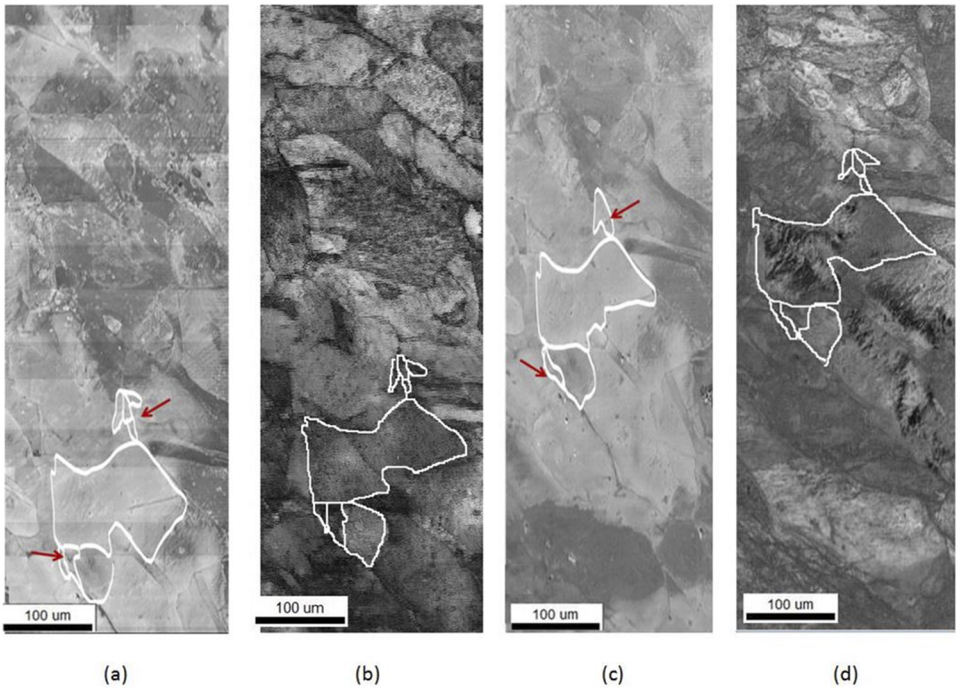

FIG. 17. (a) Thermal etching of nickel at 850 °C, SE image. (b) Corresponding EBSD image quality map. (c) SE image after cooling to room temperature; some etching remains. (d) The corresponding room temperature EBSD image quality map. Select grain boundaries have been outlined in white.

red arrows, where the grain boundaries of smaller grains are lost. However, in the EBSD images, sub-grains are still visible. Thus, it appears that the sub-grain boundaries disappear from the SE image during cooling but the sub-grains remain (see highlighted boundaries in Fig. 17). Previously, thermal etching observed post cooling has been assumed to represent the grain boundaries that form at elevated temperatures. However, the data here, highlighted in Fig. 17, suggest that thermal etching is best used for *in situ* studies as data obtained after cooling may not accurately reflect the grain structure at temperature, with the loss of visibility of etched grain boundaries in smaller grains.

V. CONCLUSIONS

The EBSD and SE images in this study demonstrate the ability to consistently image within an SEM at temperatures up to 850 °C using a novel heat stage without the need for shielding or detector modification.

Furthermore, the results presented in this paper illustrate some of the advantages and new experimental data that can be gained from *in situ* high temperature imaging. In particular, the SE images of nickel enabled observation of thermal etching formation at temperature. A comparison between images at 850 °C and room temperature post cooling indicates that when room temperature imaging is used to re-examine materials after thermal etching, there can be loss of visibility of grain boundaries around smaller grains, leading to a less accurate representation of the microstructure at temperature. Another advantage of the method was the ability to capture and document phase change, with the preliminary data of the steel ferrite–austenite phase change used as an example.

However, examination of both steel and nickel demonstrate the effect of material properties on imaging at high temperature. In nickel, the observed loss of EBSD image clarity between 300 °C and 400 °C is attributed to the transition of nickel from ferromagnetic to paramagnetic. It should be noted that this may lead to difficulties observing similar ferromagnetic materials around their Curie temperature. In steel, the effect was less clear owing to the phase change also occurring between 700 °C and 800 °C. In addition, steel showed a significant increase in surface roughness after exposure to elevated temperatures for a prolonged period of time (1 h). The roughness became greater than the typical depth of steel interaction volume. As a result, this impacted image quality, limiting the amount of imaging that can be performed when the material is heated for an extended time period.

In summary, this paper documents not only the stability of the beam and vacuum in the image quality and detectors in the temperature when using the newly designed heat stage but also the effects of material properties at temperature on the ability to image using EBSD. This work is part of a long-term strategy to capture *in situ* SE and EBSD data at these temperatures.

ACKNOWLEDGMENTS

The authors acknowledge funding from EPSRC under the iCASE scheme (Grant No. EP/R512333/1; Award Reference No. 1939581). We also thank Deben UK Ltd. for providing both financial and technical support, Marzena Tkaczyk for all her help operating the equipment in the LIMA microscopy suite, and the technicians in the Solid Mechanics group workshop at Oxford University for producing specimens. Without the above mentioned, this research would not have been possible.

DATA AVAILABILITY

The data that support the findings of this study are available within the article.

REFERENCES

[1]I. Lischewski, D. M. Kirch, A. Ziemons, and G. Gottstein, "Investigation of the α−γ−α phase transformation in steel: High-temperature *in situ* EBSD measurements," Texture, Stress, Microstruct. **2008**, 1.

[2]B. Schmid, N. Aas, Ø. Grong, and R. Ødegård, "*In situ* environmental scanning electron microscope observations of catalytic processes encountered in metal dusting corrosion on iron and nickel," Appl. Catal., A **215**, 257–270 (2001).

[3]B. Schmid and N. Aas, "High-temperature oxidation of iron and the decay of wüstite studied with *in situ* ESEM of Wu," Oxid. Met. **57**, 115–130 (2002).

[4]C. Kerisit, R. E. Logé, S. Jacomet, V. Llorca, and N. Bozzolo, "EBSD coupled to SEM *in situ* annealing for assessing recrystallization and grain growth mechanisms in pure tantalum," J. Microsc. **250**, 189–199 (2013).

[5]D. M. Kirch *et al.*, "Laser powered heating stage in a scanning electron microscope for microstructural investigations at elevated temperatures," Rev. Sci. Instrum. **79**, 043902 (2008).

[6]T. Fukino and S. Tsurekawa, "*In-situ* SEM/EBSD observation of α/γ phase transformation in Fe-Ni alloy," Mater. Trans. **49**, 2770–2775 (2008).

[7]G. Zijlstra, M. S. B. van Daalen, D. I. Vainchtein, V. Ocelík, and J. T. M. De Hosson, "Interphase boundary motion elucidated through *in-situ* high temperature electron back-scatter diffraction," Mater Des. **132**, 138–147 (2017).

[8]E. Alabort *et al.*, "*In-situ* high-temperature tensile testing of a polycrystalline nickel-based superalloy," Mater. High Temp. **33**, 338 (2016).

[9]G. Gregori, H. Kleebe, F. Siegelin, and G. Ziegler, "*In situ* SEM imaging at temperatures as high as 1450 °C," J. Electron Microsc. **51**, 347–352 (2002).

[10]G. G. E. Seward, D. J. Prior, J. Wheeler, S. Celotto, D. J. M. Halliday, R. S. Paden, and M. R. Tye, "High-temperature electron backscatter diffraction and scanning electron microscopy imaging techniques: *In-situ* investigations of dynamic processes," Scanning **24**, 232–240 (2006).

[11]Division, M. A. Welcome to OIM Data Collection.

[12]S. I. Wright, M. M. Nowell, R. de Kloe, P. Camus, and T. Rampton, "Ultramicroscopy electron imaging with an EBSD detector," Ultramicroscopy **148**, 132–145 (2015).

[13]W. Wisniewski and C. Rüssel, "An experimental viewpoint on the information depth of EBSD," Scanning **38**, 164 (2015).

[14]J. Goldstein *et al.*, *Scanning Electron Microscopy and X-Ray Microanalysis* (Springer, 2018).

[15]P. Hovington, D. Drouin, and R. Gauvin, "CASINO: A new Monte Carlo code in C language for electron beam interaction—Part I: Description of the program," Scanning **19**, 1–14 (2006).

[16]N. Brodusch *et al.*, "Imaging with a commercial electron backscatter diffraction (EBSD) camera in a scanning electron microscope: A review," J. Imaging **4**, 88 (2018).

[17]EDAX, A. M. A. D. OIM Academy Tilburg Manual.

[18]S. Kidder and D. Prior, "Reversed scan direction reduces electron beam damage in EBSD maps," J. Microsc. **255**, 89–93 (2014).

[19]A. M. Howatson, P. G. Lund, and J. D. Todd, *Engineering Tables and Data* (Springer, 2009).

[20]P. Weiss and R. Forrer, "Aimantation et phénomène magnétocalorique du nickel," Ann. Phys. **10**, 153–213 (1926).

[21]B. Legendre and M. Sghaier, "Curie temperature of nickel," J. Therm. Anal. Calorim. **105**, 141–143 (2011).

[22]See https://www.britannica.com/science/ferromagnetism for Ferromagnetism | physics | Britannica.

[23]M. M. Nowell, R. A. Witt, and B. W. True, Microscopy and Microanalysis **11**(S02), 44–48 (2005).

[24]W. W. Mullins, "Theory of thermal grooving," J. Appl. Phys. **28**, 333 (1957).